ELSEVIER

Thin optic constraint

Mireille Akilian*, Craig R. Forest, Alexander H. Slocum, David L. Trumper, Mark L. Schattenburg

Massachusetts Institute of Technology, Cambridge, MA 02139, United States

Abstract

The success of using thin substrates in various fields has urged researchers to further study the possibilities of improving the technology for future applications. For example, the high surface-area-to-weight ratio and strength of sheet glass allow flat-panel display technology to result in high-definition televisions that can be hung on walls like paintings. Sheet glass is also the prime candidate for grazing-incidence foil-optic X-ray telescopes, such as the segmented mirror approach considered for the NASA *Constellation X* mission, where cost limitations necessitate lightweight substrates.

The effects of different parameters present during the metrology of thin optics, such as gravity, frictional and thermal forces, are identified and analyzed. These forces alter the optic's surface topography by tens of microns depending on how the optics are manipulated and constrained. This renders metrology and thus surface shaping process results inconclusive.

A metrology truss utilizing monolithic flexures to kinematically constrain thin optics during metrology is designed. This device mitigates the effects of the forces mentioned above that are induced on the thin sheet while being mechanically constrained, thus significantly improving the repeatability of the optic surface map measurements.
© 2006 Elsevier Inc. All rights reserved.

Keywords: Thin optics; Monolithic flexures; X-ray telescopes; Flat panel displays; Air bearings; Surface metrology

1. Introduction

Accurately measuring and maneuvering progressively thinner (length/thickness > 10) substrates is an increasing challenge. Thin glass sheets are used in various fields including optoelectronics, the hard-disk drive industry, photomasks in the semiconductor industry, and hard pellicles for 157 nm lithography [1]. Perhaps the most important industrial application for sheet glass is the high-performance flat panel displays used in portable computers, pocket televisions, cellular phones, and high-resolution monochrome workstation displays [2]. The surfaces of such sheets must be shaped to tight tolerances, and the sheets must be mechanically maneuvered and assembled without substantial distortion to provide optimal performance.

X-ray telescopes utilizing thick, monolithic mirrors have accelerated the progress of modern astrophysics due to their excellent resolution; however, their overall performance suffers from weight and cost disadvantages. A proposed alternative approach to making high-resolution X-ray telescopes is the use of thousands of segmented thin optics, such as glass or silicon substrates, as mirrors and gratings because of their low mass and high strength [3]. The required surface figure error for each optic is less than 0.5 µm over an area of 140 mm × 100 mm, to provide a resolution comparable to that of the monolithic optic approach. Over the past several years, progress has been made in the repeatable and accurate assembly of the thin foils that provide X-ray reflecting mirror surfaces. An enabling technology for further improvements lies in the advances of surface metrology of these optics. A deep-UV Shack-Hartmann metrology system has been created to measure the flatness of the front surface of the optics, which are opaque at deep-UV wavelengths [4]; the challenge lies in constraining the thin optics with minimal distortion to measure their true surface topography.

The dominant forces that lead to the distortion of thin substrates, and thus to inaccurate metrology results, are gravity, friction during optic manipulation, and thermal stresses due to the

* Corresponding author. Tel.: +1 617 253 9342; fax: +1 617 452 2888.
 E-mail address: makilian@mit.edu (M. Akilian).
 URL: http://snl.mit.edu (M. Akilian).

difference between the coefficients of thermal expansion (CTE) of the optic and the constraining device. We discuss how thin materials such as silicon and glass wafers deform, and how they can be constrained to minimize these effects. Both analytical calculations and finite element analyses (FEA) are utilized to understand the effects of gravity on foil deformation while varying parameters such as foil thickness and angle of inclination. Friction forces imparted during foil manipulation are also studied. These theoretical analyses lead to functional requirements for the design of a holder that can be used to measure the free-form surface of thin substrates, such that the maximum deformation of the optic surface due to the shaping processes, external forces, and the repeatability of the metrology tool, is less than 0.5 μm.

2. Modeling

Various parameters play an important role in the final shape of a thin optic while constrained. In the following analyses, the effects of gravity for given pitch angles and foil thicknesses, and friction in a given assembly scheme, are analyzed.

2.1. Gravity sag

A horizontal, simply-supported optic has a maximum deformation, δ_{max}, at its center due to gravity, as given by [5]

$$\delta_{max} = \frac{\alpha \rho g \sin \theta L^4}{E t^2},\tag{1}$$

where α is a constant depending on the length-to-width ratio of the plate, ρ is the density, g is the gravitational acceleration, θ is the angle from the vertical at which the optic is held, L is the length of the optic, E is Young's modulus, and t is the optic thickness. For 100 mm × 140 mm × 0.4 mm silicon and glass wafers, the deformations due to gravity are 50 and 93 μm, respectively. A 0.5 μm flatness tolerance does not allow for this type of constraint. FEA can be used to remove gravity sag after measuring the surface of a horizontally placed optic; however, the accuracy of this method is strongly dependent on the optics' homogeneity, thickness uniformity, and placement repeatability. Rectangular glass used for flat panel displays and X-ray telescopes has a total thickness variation of ±20 μm. The change in surface deformation for a 0.4-mm thick optic with the quoted thickness variation, using Eq. (1), is between −0.75 and 0.85 μm, which is beyond the required 0.5 μm tolerance.

2.1.1. Gravity sag as a function of pitch

Orienting the optics vertically effectively reduces the gravity-induced sag. Deformation of a simply-supported, 100 mm × 140 mm × 0.4 mm glass wafer as a function of pitch angle is shown in Fig. 1. This plot helps define the thin optic holder functional requirements. Specifically, if we allocate 15% of the allowable peak-valley (P-V) error (0.5 μm) to pitch angle repeatability, this repeatability should be $100''$ at worst. The corresponding ∼70 nm glass sheet deformation should not significantly compromise the assessment of the manufacturing quality.
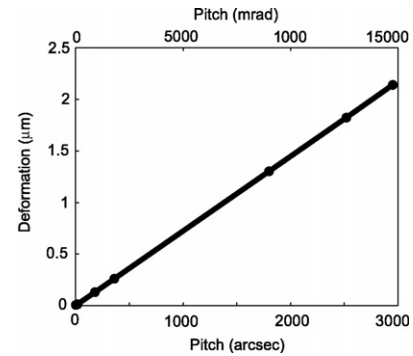

Fig. 1. Maximum glass foil deformation as a function of pitch angle for a 140 mm × 100 mm × 0.4 mm optic with ball and socket boundary conditions at three constraint points: two at the bottom and one at the top.

2.1.2. Gravity sag as a function of thin optic thickness

The thickness of the thin optic affects the tolerance to inclination errors. Eq. (1) reveals that the deformation is inversely proportional to the thickness squared. Using FEA, Fig. 2 shows the relationship for an optic held at 0.82° ($2952''$) from the vertical. A 400 μm thickness has been chosen for the telescope foils, balancing the needs for low mass and relatively small deformations.

2.2. Friction

Friction between the thin optic and the constraining fixture can cause intolerable distortion. An assembly scenario, where a thin optic is slid into position by finger-like microstructure combs, in accordance with other assembly research [6], is shown in Fig. 3(a). Comb teeth provide the actuation force initiating friction that arises from contact between the optic and comb base. Modeling the thin optic as shown in Fig. 3(b), the friction force, $F_{friction}$, is

$$F_{friction} = \mu m g,\tag{2}$$

where μ, the coefficient of static friction, has been measured to be 0.39 [7]. The glass sheet mass, m, is 14.1 g. The comb and glass sheet dimensions are such that $a = 1.09$ mm and $l =$
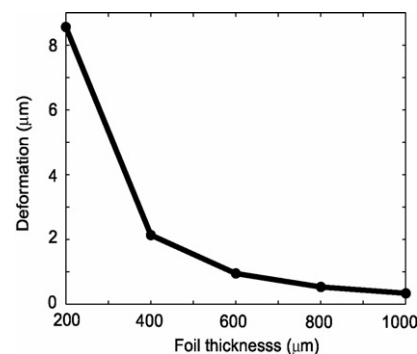

Fig. 2. Maximum glass foil deformation as a function of thickness for a 140 mm × 100 mm optic held at 0.82° from the vertical with ball and socket boundary conditions at three constraint points: two at the bottom and one at the top.
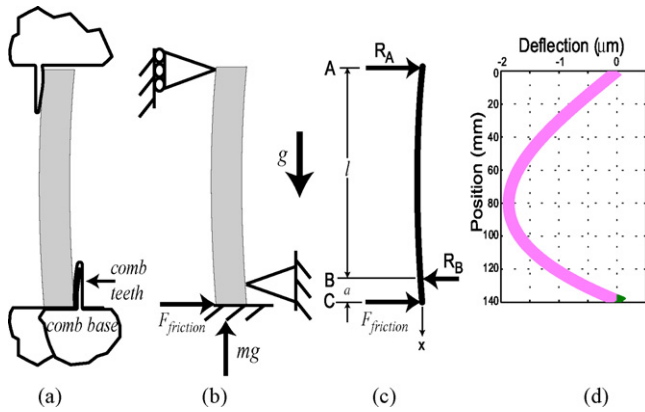
Fig. 3. Forces from comb actuation and friction at the bottom of the foil can lead to distortion.

138.91 mm. The maximum glass substrate deflection, δ_{max}, is

$$\delta_{max} = \frac{F_{friction}a^2(l+a)}{3EI} = 1.9\,\mu m. \tag{3}$$

An FEA simulation with a ball-socket triad as boundary conditions gives $2.76\,\mu m$. Experiment shows this value to be $2.01\,\mu m$. This is beyond required tolerances; therefore, the constraining device must reduce the effect of friction on the optic.

3. Concepts

Different methods for mounting and constraining thin optics have been considered for this device, ranging from mounting the optic horizontally and using FEA to remove gravity sag, to mounting the optic vertically and constraining it either on one face or both by using a variety of flat air bearings, vacuum preloaded air bearings, and flexures to inherently eliminate gravity effects and reduce the deformations caused by friction and thermal stresses. The strengths and weaknesses of individual concepts are studied and further elaborated in [8].

The most promising mounting concepts have the optic held vertically and approached from both sides. In order to choose between having actual contact with the optic and the constraining tool by using flexures or avoiding contact, by using air bearings, both concepts have been analyzed, tested, and evaluated.

3.1. Double-sided air bearings

This approach constrains the optic without having contact with its two faces. Air bearings are used to constrain five degrees of freedom of the optic, as shown in Fig. 4. Three pairs of 7 mm-diameter opposing air bearings are used to constrain x translation and y and z rotation. Two horizontal vacuum preloaded air bearings are used to constrain z translation and x rotation.

The plane formed by the three air bearings on one side of the optic is placed close to the vertical to decrease deformation associated with gravity sag. These reference bearings are shown behind the optic in Fig. 4. Mobile air bearings are placed on the opposite side of the optic. These bearings can be moved back and forth with respect to the optic face to facilitate insertion/removal of the optic and to provide the necessary preload to keep the optic
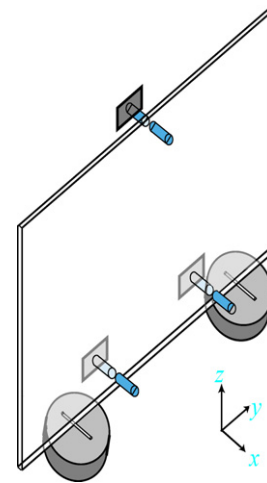

Fig. 4. Three pairs of opposing air bearings constraining x translation and y and z rotation, and two vacuum preloaded air bearings constraining z translation and x rotation. The bearings at the front surface of the optic can be moved back and forth to facilitate inserting the optic into the device.

in place once it is mounted into the device. Because there is no contact with the optic's surface, this strategy allows for thermal expansion mismatch between the optic and the device, while eliminating Hertzian contact and non-repeatable friction forces. The load on these bearings is very small, since the optic is held vertically.

Hammer instability if present could be catastrophic. The role of these bearings is mainly to constrain translation in one direction but allow for rotation or tilt to avoid overconstraining the optic. Inherently compensated air bearings have been chosen for this initial experiment, since their stability is superior to annular or pocket bearings [9], and their manufacturing is simpler; however, using different configurations could provide better preload and stiffness if hammer instability is controlled by optimizing different parameters, such as inlet hole diameter, outer diameter, supply pressure, etc. Detailed work has been done by Fourka and Bonis [10], Stiffler [11], and Mori [12] to study the effects of such parameters on the performance of inherent, pocket, annular, and porous bearings.

Detailed analysis and description of the mechanism for this concept is found in [8]. The double-sided air-bearing strategy has the advantage of constraining the optic without surface damage caused by contact forces; however, the complexity associated with the design and assembly of air bearings is a major drawback on the overall concept. In addition, local torques on the surface of the thin optic result from offset forces on both sides if the opposing bearings are not exactly aligned facing each other. This results in errors in the optic surface topography. Aligning the bearings has been found to be quite challenging.

3.2. Flexure assembly

This concept basically replaces the thin layer of air in the previous concept with compliant mechanisms, as shown in Fig. 5, to decrease frictional and thermal stresses on the optic. The length of the flexures used is to be kept at a minimum to avoid the overall bulkiness of the tool, yet the flexures have to be compli-

The second concept utilizing flexures to constrain thin optics mitigates the problems with friction and thermal stresses but does not completely eliminate them. On the other hand, the design, machining and assembly of the flexures is much simpler and cost effective. The overall stability and stiffness of this system are superior to those of the air bearing device. The tool can impose errors on the surface of the optic if not used properly; yet, the flexure assembly is designed such that the maximum error obtained is less than the required tolerance of 500 nm surface flatness. However, contact at the edges of the optic is unavoidable; this may become a problem when the entire surface of the optic is covered with sensitive nanostructures susceptible to Hertzian stresses, a problem not found in the case of air bearings.

4. Design details of flexure assembly

The sections that follow present details of the design parameters followed to constrain 100 mm-diameter circular optics and 100 mm × 140 mm rectangular optics.

4.1. Double-sided flexures

Three double-sided flexures approach the optic from both sides, as shown in Fig. 6. These flexures are themselves divided into two parts, as shown in Fig. 7: the vertical arm which can be pulled open to facilitate the insertion and removal of the thin optic into the device and provides the required preload once the optic is in position, and the opposing flexures, which account for thermal expansion mismatch between the optic and the device. Fig. 7 shows a thick, stationary arm parallel to the vertical one. The three ruby balls individually attached to these thick arms form the plane in which the front surface of the optic lies.

The material of choice is stress-relieved aluminum 6061-T651 for its high-yield stress-to-Young's-modulus ratio, ease of machining, availability, and low cost. These flexures have been manufactured using wire-electric-discharge machining (wire EDM) of a monolithic part to avoid any misalignment between the opposing arms that would lead to local torques on the optic and result in unacceptable surface deformations. This manufacturing process obligates the use of blade flexures compliant in one direction, rather than circular ones, which are compliant in all directions.

A block made of nickel-coated aluminum, optically polished to 100 nm flatness, is used as a reference for comparison with the surface of the thin optics. The double-sided monolithic flexures are attached to this block by means of a vertical tilt stage, as shown in Fig. 5. The whole device sits on a horizontal tilt stage with three fine-threaded screws to control the pitch and yaw of the tool with the aid of an inclinometer, which sits on top of the reference block. The inclinometer has a resolution of 18″ with a repeatability of 36″ in both pitch and yaw [16], which meets the 100″ requirement, and is used to monitor and compensate for angular changes during metrology.

The vertical stage which carries the monolithic, double-sided flexures is also controlled by means of three fine-threaded screws to align the front surface of the optic with the surface of
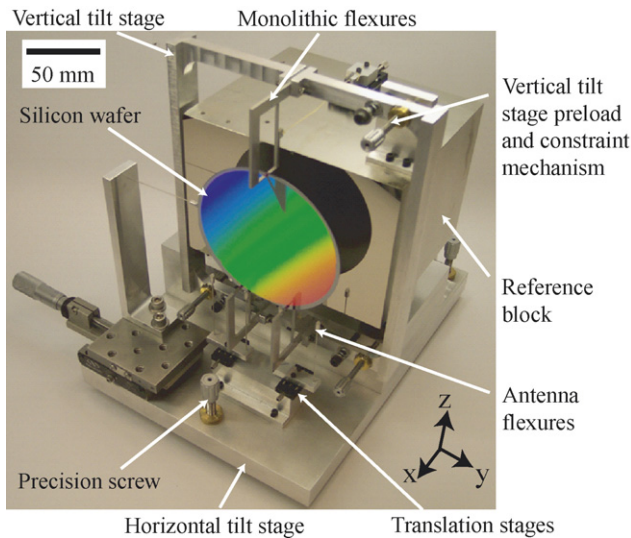

Fig. 5. The metrology truss utilizing monolithic double-sided and tube flexures to constrain thin circular and rectangular optics during surface metrology.

ant enough to accommodate external forces. The misalignment between the opposing flexures is a major concern as well, similar to the air bearing case. Wire-electric-discharge machining is chosen to make the opposing flexure arms out of a monolithic part to minimize misalignment error rather than using individual opposing flexures. This method is advantageous, since it guarantees the alignment of the two arms, thus minimizing associated errors, and it introduces minimal forces on the flexures during machining when compared to other methods of manufacturing, such as regular machining or water-jet machining, which improves the overall accuracy of the dimensions and geometry of these flexures.

These monolithic flexures constrain translation along the *x* direction and rotation about the *y* and *z* directions. Two "antenna" flexures composed of long hollow tubes carry the load of the optic while constraining rotation about the *x* direction. These antennas help while positioning the optic into the device, since the forces they impart on the optic as it is being adjusted to its final position are very small.

3.3. Comparison between air bearings and flexures for constraining thin optics

Although air bearings ideally provide better performance when constraining thin optics without distorting their shapes [13], flexures have been chosen to build the device used to hold wafers during metrology. Air bearings require extremely flat and smooth surfaces with critical assembly and tight tolerances, which increase the cost of the device. The risk of failure caused by pressure variations in the system is high. This in turn leads to a change in the critical pitch angle or imbalance of the optic. The need for numerous pressure and vacuum lines restrains the mobility of the device and adds to the intricacy of the assembly. Finally, the lateral stability of the load-carrying vacuum-preloaded thrust bearings floating against a horizontal, flat surface needs to be further addressed.
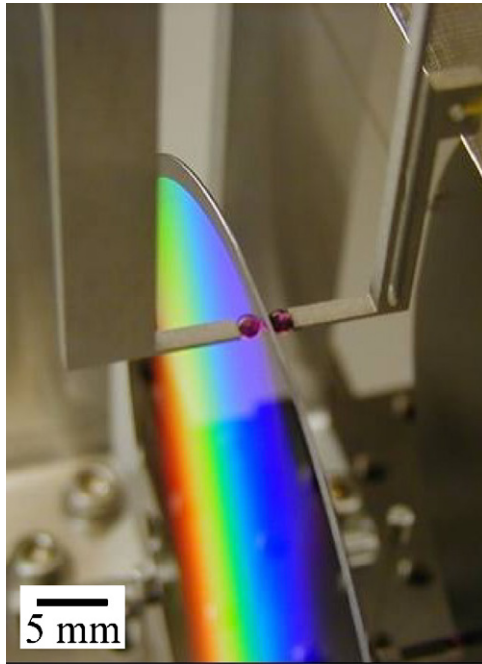
Fig. 6. The constraint of a silicon wafer with a 400 nm spatial period grating by monolithic double-sided flexures, with two ruby balls mounted at the tip of the opposing arms to form a point contact with the optic.

the reference block to a repeatability of 0.25″ and 2.3″ in pitch and yaw, respectively. The alignment between the two surfaces is performed using an autocollimator with a resolution of 0.021″.

4.1.1. Vertical flexure arm

The vertical flexure is designed to have a horizontal displacement of 1.6 mm at its tip, with a maximum stress of 145 MPa, which corresponds to 52% of the yield stress of aluminum. This deflection is needed for inserting the optic between the opposing flexure arms. Since a single blade is used for this flexure,
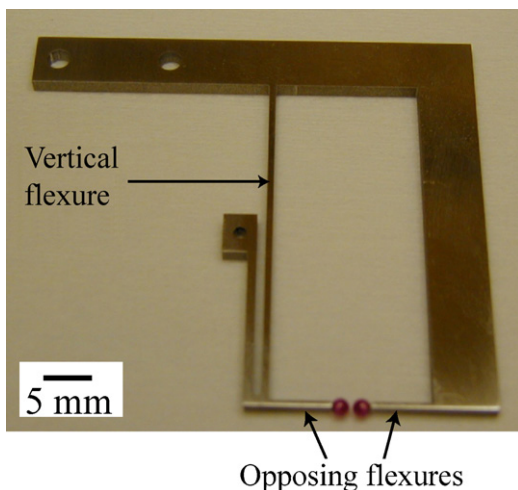

Fig. 7. Monolithic, wire-EDM cut, double-sided flexures made of stress-relieved aluminum 6061-T651 with ruby ball tips. The left vertical arm is actuated back and forth from its center to allow for the optic insertion/removal. The opposing flexures accommodate thermal expansion mismatch between the optic and the aluminum device.
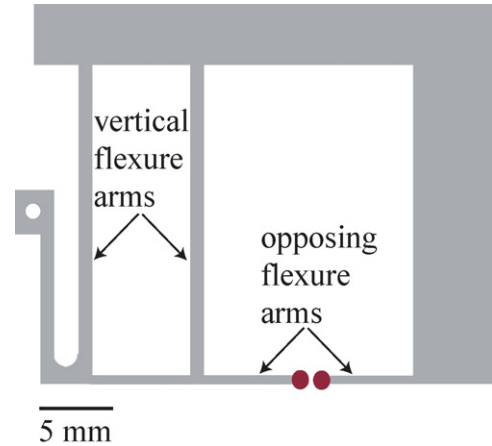

Fig. 8. Monolithic flexure using two vertical arms actuated halfway through their length to eliminate angular and vertical errors.

horizontal displacements of the tip are accompanied by vertical displacement and pitch angle errors as well. Using FEA, it is determined that these errors are smallest when the flexure is actuated at its midpoint, as shown in Fig. 7. The value of the vertical error motion decreases as the length of the flexure is increased and the horizontal displacement is decreased. Though small, this vertical displacement causes a slight offset between the arms, whose effect was found to be much smaller than the design requirements. The angle error on the other hand can be more of a problem, since the length of the opposing arm attached perpendicularly to the vertical arm results in a sine error [8], or an additional vertical error, as described in the next section. This places an upper limit on the length of the opposing flexure arms, if misalignment between the two is to be kept at a minimum, to avoid the presence of local torques on the surface of the optic. If a tighter tolerance is needed, two sets of blades can be used for the vertical arm instead of one, as shown in Fig. 8. When actuated at the length midpoint of these blades, there will be no bending moment at their tips and as a result, no pitch angle errors. The vertical error motion, though still dependent on both flexure length and horizontal displacement, is reduced [9].

After the optic is in position, all three vertical flexure arms situated at different positions on the optic surface must equally preload the optic; therefore, a string attached to a linear translation stage on one end and at halfway the length of the vertical arm on the other end, is pulled to open the arm and loosened to close it. Once contact with the optic is achieved, the string tension vanishes, and the flexure, with dimensions shown in Fig. 9, acts as a cantilever with a stiffness k of 2.45×10^{-4} N/μm, as given by

$$k = \frac{3EI}{L^3}. \tag{4}$$

Upon placing the 0.4-mm thick optic into the device, the flexure arm is displaced by 275 μm from its original position, which corresponds to a restoring force of 0.067 N. The fact that this preload force is small poses a risk on the overall stability of the device. Tests have shown that this does not manifest itself as a problem, and the optic does not vibrate while constrained; however, the countermeasure is to resize the dimensions of the
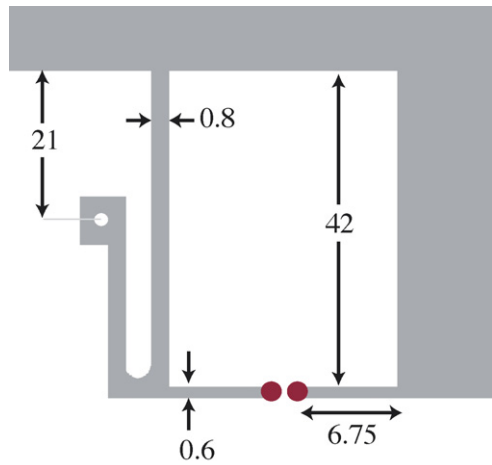
Fig. 9. Monolithic flexure dimensions in mm. The width of the flexure is 2 mm into the page. The ruby balls at the opposing flexure tips are 2 mm in diameter.

vertical flexure to increase its stiffness but result in a smaller opening during optic insertion into the device.

4.1.2. Opposing flexure arms

Blade flexures are compliant in only one direction, whereas thermal expansion occurs in all directions; therefore, the blade flexures must be held at different angles for best stability and performance. Blades have been chosen to allow wire-EDM manufacturing for reasons mentioned before. The flexures in this design have been laid out such that the normals to the blades of the flexures bisect the angles of the triangle formed by the three contact points with the optic, as shown in Fig. 10(a). This is analogous to the well known kinematic coupling design for best stability, where the couplings constrain the carried load in all directions [9]. The top flexure is the most susceptible to thermal mismatch errors because the differential length between the optic and the device is a maximum at this point; therefore the blade of the top flexure is placed such that its compliance is along the direction of maximum thermal growth. A better lay out for these flexures takes the load-constraining flexures into consideration as well. In other words, the normals to the blades, which define the directions of the blades' degrees of freedom, intersect with the perpendiculars to the load-carrying flexures at one point. Fig. 10(b) shows such a configuration. The effect of the thermal gradients for the lay out used in the current design is described in Section 5.

The tips of the opposing flexures have a post used for mounting drilled, 2 mm-diameter ruby balls. Contact occurs between the ruby balls and the optic. Ruby is chosen for its hardness, which implies better repeatability and small Hertzian deformation of 76 nm for the given preload on 0.4 mm thick wafers; however, Hertzian forces occur on both sides of the optic, canceling each other out with negligible effect on the overall surface topography. The point of contact between the ruby and the substrate is near the edges of the substrate; therefore, nanostructures covering the substrate are left intact except at the three points of contact.

The condition of no slip at the interface is assumed when calculating the required stiffness for the opposing arms, which are
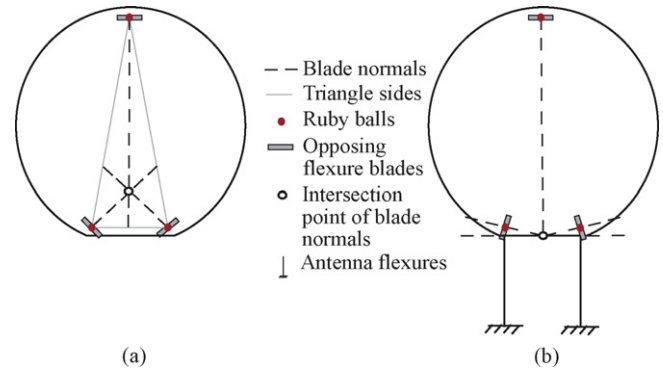

Fig. 10. (a) Flexure blades placed such that the normals to these blades bisect the angles of the triangle formed by the three contact points between the circular optic and the ruby balls. (b) Flexure blades placed such that all flexures' degrees of freedom intersect at one point.

modeled as cantilevers. The force at the tip of these cantilevers is the friction force between the ruby ball and the glass surface for the 0.067 N preload. For a coefficient of friction of 0.3 between ruby and glass [14], the resulting friction is 0.02 N. A limit of 1 °C temperature change per reading controls the differential change between the aluminum housing and the glass optic, which represents the deformation required per flexure depending on its spatial position. The flexures are placed at characteristic thermal lengths of 100 and 17 mm; therefore, a 1 °C temperature change leads to 1.2 and 0.27 μm differential changes in length at both positions, respectively. The corresponding required flexure stiffness ranges between 0.017 and 0.095 N/μm.

The dimensions of the opposing arms shown in Fig. 9 are chosen to minimize the parasitic motion discussed earlier and to facilitate the machining process. The resultant stiffness is 0.024 N/μm. The overall vertical error motion is found to be 6.6 μm using FEA. To determine the effect of this error, the optic is modeled as a simply-supported beam with twin loads representing the preloads from the vertical arm at an offset of 6.6 μm from the supports, as shown in Fig. 11. The resultant maximum deformation, δ, of the surface of the optic is [15]

$$\delta = \frac{Fa(3L^2 - 4a^2)}{24EI}, \tag{5}$$

where F is the preload, a is the error, $L = 91.7$ mm is the distance between the top and bottom flexures, E is Young's modulus, and I is the moment of inertia. The corresponding maximum deflection is 9 nm. This value is insignificant when compared to other major sources of error in both the device and the metrology tool.

The flexures placed at the 100 mm characteristic length are not as compliant as required to fully accommodate the thermal differential length. As the aluminum housing expands, a net force in-plane with respect to the optic, along the z direction as shown in Fig. 5, acts on both surfaces of the optic. As this force becomes larger than the static friction between the opposing ruby balls and the optic, the flexures slip along the optic surface.

The overall stiffness of the monolithic module controlling the stability of the optic during metrology depends on the axial stiffness $k_o = 12.62$ N/μm of the opposing arms, the lateral
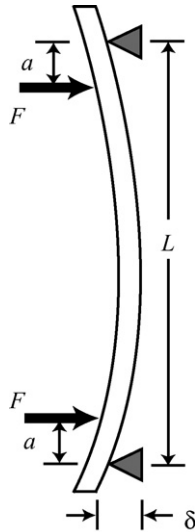
Fig. 11. Thin optic modeled as a simply-supported beam with twin loads to characterize the deflection, δ, caused by the misalignment of the ruby balls due to the parasitic motion. F is the preload of the flexure on the optic, a is the parasitic displacement, and L is the distance between the upper and lower monolithic flexures.

stiffness of the vertical arm $k_v = 2.45 \times 10^{-4}$ N/μm, and the Hertzian stiffness $k_{Hz} = 0.794$ N/μm, which is calculated using the preload force and the Hertzian deformation of the system. The overall effective stiffness k is 0.748 N/μm, as given by

$$k = \frac{k_o k_{Hz}}{k_o + k_{Hz}} + \frac{k_v k_o k_{Hz}}{k_o k_v + k_o k_{Hz} + k_v k_{Hz}}. \tag{6}$$

4.2. Load-carrying flexures

While placing the thin optic into the device, the user may apply a temporary torque, distorting the wafer surface. When placed on a rigid body, friction at the interface may hinder the internal elastic force of the optic from restoring it to its natural shape, decreasing the accuracy of the metrology results. Therefore, the load of the optic is carried by two antenna flexures, whose compliance reduces any temporary warp introduced to the optic surface by the user. These two antennas also constrain the rotation around the x axis. These flexures are made of commercially available precision stainless steel tubes. Four such antennas are present, where the inner two are 0.5 mm shorter than the outer two. This allows for the flat of the circular optics to be placed on the inner two flexures, whereas wider, rectangular wafers sit on the outer pair, as shown in Fig. 12. A 2 mm-long sapphire tube mounted on the tip of the antennas, as shown in Fig. 13, forms a line contact at the interface with the optic to facilitate its placement on the flexures. Each flexure is mounted on a linear stage to move it back and forth to accommodate different optic thicknesses. An identical flexure is used to control the position of the optic along the y direction.

In order to calculate the appropriate stiffness of these antennas, it is required to estimate the forces and deflections at their tips. Modeling the internal restoring force of the optic with different boundary conditions imposed by the user is complex. A problem with resting an optic on a rigid body arises when this

restoring force is less than the friction at the interface because the optic cannot slip; however, with the antennas, the optic natural surface can be retrieved as the flexures bend accordingly. Since the optic restoring force is unknown, friction is used as the upper limit force for calculating the required stiffness for the antennas; therefore, the design antenna stiffness must be smaller than the value calculated using friction as the force. Friction between the sapphire tube on the antenna and the glass optic is calculated using the weight of the optic, 0.138 N, equally divided between the two antenna flexures, and the coefficient of static friction between sapphire and glass [14]. The resulting friction is 0.024 N per flexure. The maximum distance that the optic may move after it has been placed onto the antennas is controlled by the distance of 1.4 mm between the two ruby balls after one has been retracted. Subtracting the thickness of the 0.4 mm of the wafers from this opening, the total distance that the optic may move is 1 mm. In reality, the surface errors introduced by the user are smaller than 1 mm, in other words, the flexures will actually have to deflect by an amount less than 1 mm; therefore, using 1 mm for the deflection of the tip of the antenna is a conservative value. The design stiffness is found to be 2.36×10^{-5} N/μm.

Another property of these flexures is their load-carrying capacity. A thick, flat mirror is required to align the plane of the reference ruby balls with a reference surface. Such optics with a flatness of 1/4 wave, and a weight of 0.6 N are carried by the antennas. The load capacity of the antenna flexures is calculated using Euler's equation for beam buckling. The flexures are 50 mm long with an outer diameter of 0.635 mm and an inner diameter of 0.508 mm. The actual stiffness of the flexures is
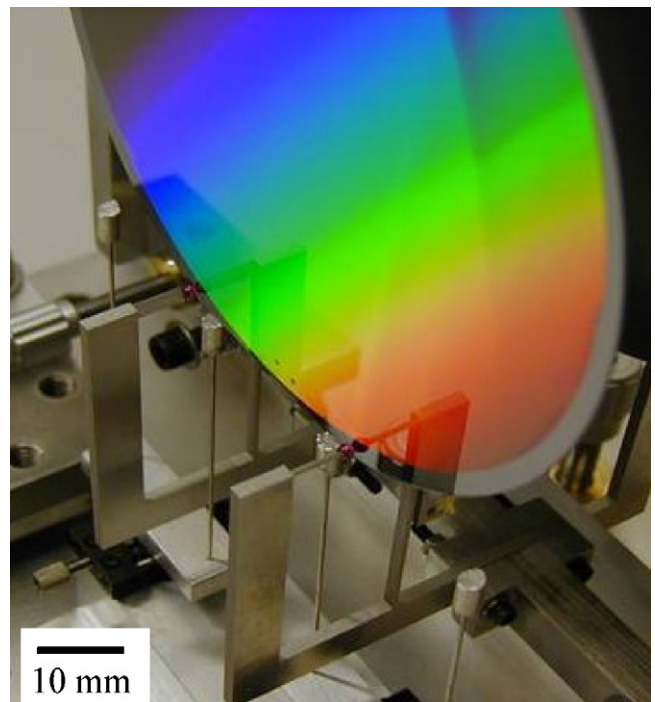

Fig. 12. Circular optics sit on the inner pair of antenna flexures, whereas rectangular ones contact the outer, longer pair. This configuration allows for better stability with the rectangular optics, since the corresponding flexures are placed further apart; the length of the flat on circular optics (around 31 mm) constrains the distance between the inner flexures.

2.18×10^{-5} N/μm, which is less than the upper limit of stiffness calculated earlier, and the load capacity is found to be 0.82 N, which is greater than the weight of the thick, flat mirrors.

The accurate placement of the optics with respect to the stationary ruby balls, which determine the plane of metrology, is critical. If the lower edge of the optic is placed away from the lower stationary ruby balls, then as the optic is pushed by the vertical arm, to be fully constrained and ready for metrology, the load-carrying flexures bend to translate the optic to its final position; however, the finite stiffness of the flexure induces a restoring force at the lower edge of the optic, which leads to its deformation. Fig. 14 shows the worst case, where the optic is placed at a distance 1 mm away from the stationary ruby balls. To estimate this deformation, the optic is modeled as an overhung, simply-supported beam with a force of $2F$ at one free end, where F is the force from every flexure. The maximum force associated with the 1 mm displacement is 0.044 N. The corresponding deflection δ_{max} is

$$\delta_{max} = \frac{Fa^2(l+a)}{3EI}, \tag{7}$$

where a is the distance along the length of the optic, between the force and the closest pin, in this case 2 mm, l is the spacing between the two pins and equals 93.4 mm, E is Young's mod-
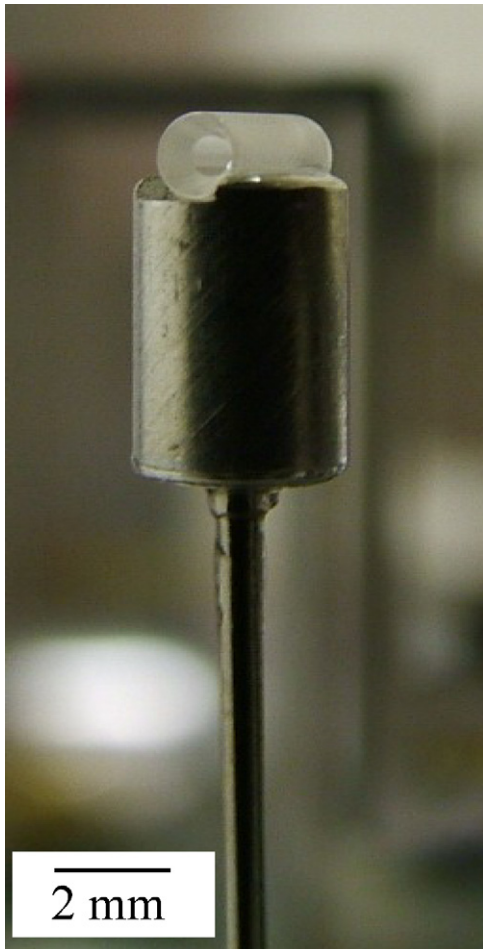

Fig. 13. Sapphire tube mounted on top of the antenna flexures to facilitate the placement of the optic on these flexures.
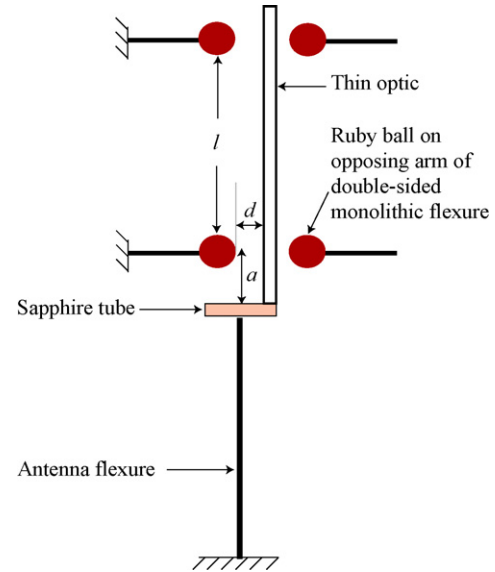

Fig. 14. Thin optic placed at the very edge of the sapphire tube on the antenna flexures. This leads to the motion of the flexures by distance d until the optic is fully constrained, resulting in a restoring spring force from the antenna flexures onto the optic.

ulus and I is the moment of inertia. The maximum deflection is estimated to be 148 nm, which can be reduced if the optic is placed close to its proper position on the load-carrying flexures. In practice, this problem is mitigated by simply placing the lower edge of the optic in contact with the stationary ruby balls, to minimize antenna-induced errors. Note that this error is much smaller than the ~2 μm error, shown in Section 2.2, from placing the optic on a rigid body as opposed to flexures.

5. Results and discussions

Several tests have been conducted to evaluate the performance of the flexures. The effect of temperature change during metrology has been studied by measuring the surface of an optic over a span of 3 h, during which the temperature of the room increases by 1.2 °C. The surface of the constrained optic has been measured using the Shack-Hartmann system [4], which has a repeatability of ~40 nm, and the results have been fitted to Zernike polynomials [17]. The maximum change in the peak to valley is found to be ~100 nm.

To demonstrate the severity of misplacing the optic onto the load-carrying flexures, the optic has been placed at the edge of the sapphire tube, as shown in Fig. 14, such that the antennas are forced to move by approximately 1 mm while the ruby balls fully constrain the optic. The resulting force from the antennas leads to a surface deformation of 94 nm.

To evaluate the performance of the tool in a real situation, a thin optic is placed on the antenna flexures, fully constrained by the ruby balls, measured, removed and placed into the tool again following the same procedure. The device repeatability is 55 nm, which is sufficient to evaluate foil manufacturing and shaping processes, where the required surface flatness for X-ray optics is < 500 nm.

The metrology truss has further been used to constrain a 0.5 mm thick, 100 mm diameter silicon wafer to evaluate its surface before and after applying magneto-rheologic finishing to flatten its surface. This optic's surface flatness has been reduced from 2.8 μm to 75 nm over an aperture of 75 mm [18].

Acknowledgments

References

[1] De Bisschop P, Kocsis M, Bruls R, Van Peski C. Initial assessment of the impact of a hard pellicle on imaging using a 193-nm step-and-scan system. J Microlithogr, Microfab Microsys 2004;3:239–62.

[2] Cable M, Parker JM. High-performance glasses. Chapman and Hall; 1992.

[3] Forest CR, Schattenburg ML, Chen CG, Heilmann RK, Konkola P, Przbylowski J, et al. Precision shaping, assembly and metrology of foil optics for X-ray reflection gratings. Proc Soc Photo-Optic Instrumen Eng 2002;4851:538–48.

[4] Forest CR, Canizares CR, Neal DR, McGuirk M, Slocum AH, Schattenburg ML. Metrology of thin transparent optics using Shack-Hartmann wavefront sensing. Optic Eng 2003;43:742–53.

[5] Roark RJ. Roark's Formulas for stress and strain. McGraw-Hill; 1989.

[6] Forest CR. X-ray telescope foil optics: assembly, metrology, and constraint. Masters thesis, Massachusetts Institute of Technology, Department of Mechanical Engineering; 2003.

[7] Mongrard O. High-accuracy foil optics for X-ray astronomy. Masters thesis, Massachusetts Institute of Technology, Department of Aeronautics and Astronautics; 2001.

[8] Akilian M. Thin optic surface analysis for high resolution X-ray telescopes. Masters thesis, Massachusetts Institute of Technology, Department of Mechanical Engineering; 2004.

[9] Slocum AH. Precision machine design. Society of Manufacturing Engineers; 1992.

[10] Fourka M, Bonis M. Comparison between externally pressurized gas thrust bearings with different orifice and porous feeding systems. Wear 1997;210:311–7.

[11] Stiffler AK. Analysis of the stiffness and damping of an inherently compensated, multiple-inlet, circular thrust bearing. J Lubric Technol 1974;96:329–36.

[12] Mori H. A theoretical investigation of pressure depression in externally pressurized gas-lubricated circular thrust bearings. J Basic Eng 1961;83:201–8.

[13] Forest CR, Akilian M, Vincent G, Lamure A, Schattenburg ML. Thin glass optic and silicon wafer deformation and kinematic constraint. Proceedings of the 18th Annual Meeting ASPE 30;2003:39–42.

[14] Automation Creations Inc. Material property data. Available at: http://www.matweb.com.

[15] Van Voorhis M. Simply supported beam with twin loads, 1999. Available at: http://ourworld.compuserve.com/homepages/MJVanVoorhis/T309.htm.

[16] Applied Geomechanics, Inc., 1336 Brommer Street, Santa Cruz, California 95062, USA.

[17] Chang C-H, Akilian M, Schattenburg ML. Describing isotropic and anisotropic out-of-plane deformations in thin cubic materials using Zernike polynomials. Appl Optics 2006;45:432–7.

[18] Heilmann RK, Akilian M, Chang C-H, Hallock R, Cleaveland E, Schattenburg ML. Shaping of thin grazing-incidence reflection grating substrates via magnetorheological finishing. In: Citterio O, O'Dell SL, editors. Proc. SPIE 5900, Optics for EUV, X-ray, and Gamma-ray Astronomy II; 2005. p. 73–80.